The metallophilic interaction between cyclometalated complexes: photobiological applications

Zhou, X.

6

Nitrogen coordination *vs.* rollover cyclometalation in tetrapyridyl anticancer gold(III) complexes

In this work, a pair of gold(III) complexes derived from the analogous tetrapyridyl ligands ***H$_2$biqbpy1*** *and* ***H$_2$biqbpy2*** *have been synthesized, i.e., the bis-cyclometalated complex* ***[Au(biqbpy1)Cl*** *(****[1]Cl****) and its isomer* ***[Au(biqbpy2)Cl*** *(****[2]Cl****). In* ***[1]$^+$****, two of the four pyridyl rings are coordinated to the metal via a Au-C bond ("rollover" coordination mode, C^N^N^C) and the two non-coordinated amine bridges of the* ***biqbpy1^{2-}*** *ligand remain protonated, while in* ***[2]$^+$*** *the four pyridyl rings of the* ***biqbpy2^{2-}*** *ligand are coordinated to the metal via an Au-N bond (coordination mode N^N^N^N), but both non-coordinated amine bridges are deprotonated. As a result, both* ***[1]Cl*** *and* ***[2]Cl*** *are monocationic, making it possible to compare the effect of bis-cyclometalation on the chemical reactivity, anticancer properties, and protein interactions of these gold(III) compounds, without a change of their overall charge. The rollover cyclometalation resulted in* ***[1]Cl*** *being coordinatively stable in biomimetic conditions, while* ***[2]Cl*** *was reduced by millimolar concentration of GSH into metastable Au(I) species ultimately releasing the free ligand* ***H$_2$biqbpy2*** *and Au$^+$ ions. On the other hand,* ***[1]Cl*** *made nanoparticles in cell-growing medium that resulted in very efficient cellular uptake. The chemical stability of* ***[1]Cl*** *in reducing conditions led to decreased thioredoxin reductase (TrxR) inhibition properties, compared to* ***[2]Cl****, which released the known TrxR-inhibiting Au$^+$ ions. On the other hand,* ***[1]Cl*** *had more selective anticancer properties, i.e. it was almost 10 times more cytotoxic to human cancer cell lines (A549, A431, A375, MCF7) than to a non-cancerous cells line (MRC5). Both complexes* ***[1]Cl*** *and* ***[2]Cl*** *displaced reference radioligand [^{3}H]dofetilide equally well from cell membranes expressing the K$_v$11.1 (hERG) potassium channel, and more so than the tetrapyridyl ligands* ***H$_2$biqbpy1*** *and* ***H$_2$biqbpy2****. Overall, these results suggested that bis-cyclometallation is an appealing method to improve the redox stability of Au(III) compounds. Such stability improves their selectivity against cancerous vs. non-cancerous cells, possibly due to their interaction with the K$_v$11.1 potassium channel.*

This chapter will be submitted as a full paper: X.-Q Zhou, I. Carbó-Bagué, M. A. Siegler, J. Hilgendorf, U. Basu, R. Liu, A. P. IJzerman, I. Ott and S. Bonnet*, *JACS Au*.

6.1 Introduction

The discovery of cisplatin's anticancer activity has brought a new era for the bioinorganic and medicinal chemistry communities.[1] Nowadays, cisplatin is one of the main chemotherapeutic drugs for the treatment of various cancers. However, the corresponding *trans* isomer, trans-$[Pt(NH_3)_2Cl_2]$ is clinically inefficient, which is attributed to its much lower efficiency to form cross-link DNA adducts.[2] Overall, the anticancer properties of a metal compound can be strongly influenced by the intrinsic (stereo)chemical differences between two isomers.[3] Recently, establishing structure-activity relationship between isomers of the same molecule has emerged as a new frontier in bioinorganic medicinal chemistry.[4, 5]

Next to platinum itself, many heavy metal complexes are being investigated for their potential anticancer properties. They may show different modes of action (MOA), such as DNA binding, disruption of membranes, enzyme inhibition, or reactive oxygen species generation, which allows in many cases to overcome the resistance of tumors to cisplatin.[6-8] In particular, gold complexes have been considered as an alternative to platinum because of the specific affinity of gold(I) ions for the thiol groups present in many biomolecules, especially thioredoxin reductase (TrxR) and glutathione (GSH).[8-10] The TrxR/GSH system and its different components have been reported as the major cellular line of defense against increased oxidative stress and the accumulation of reactive oxygen species (ROS); when it works properly, it helps the cell to stay alive. Meanwhile, the expression of these two biomolecules is known to be higher in cancer cells than in normal cells, as the former need to sustain higher metabolism than the latter.[11, 12] Altogether, the TrxR/GSH system has been recognized as a good target for anticancer therapy, notably for gold prodrug candidates. For example, Auranofin, an Au(I) compound characterized by the coordination of a phosphine and a thiol ligand in a linear arrangement, has been clinically approved for the treatment of rheumatoid arthritis for years. More recently, it has been thoroughly investigated as an anticancer drug, for its significant inhibition properties towards TrxR.[13] Next to Au(I), many Au(III) compounds have been evaluated as anticancer drugs,[14] many of them based on polypyridyl ligands. Interestingly, polypyridyl Au(III) complexes are typically reduced to Au(I) species upon cellular uptake, which is often accompanied by the release of the polypyridyl ligand(s).[10, 14] Some Au(III) polypyridyl complexes are also reactive to the thiol residue of human serum albumin, leading to the dissociation of the complex before it reaches cancer tissues. By contrast, cyclometalated Au(III) complexes, *i.e.* compounds that have at least one metal-carbon σ bond, have been considered because of their higher redox stability in physiological conditions.[10] On the other

hand, cyclometalation typically reduces the positive charge of Au(III) complex, which can strongly modify its biological properties, notably its cellular uptake and/or interaction with serum proteins.[15]

Most cytotoxic, cyclometalated Au(III) complexes known to date are based on the combination of a bipyridine or terpyridine ligand and monodentate ligand(s), [14, 15] while cyclometalated Au(III) complexes based on tetradentate ligands are rare.[15] Among the different reactions available to prepare cyclometalated complexes, an unconventional one called "rollover" has been identified in recent years, in particular in catalysis where the uncoordinated nitrogen atoms can play an important role.[16] Rollover cyclometalation is a specific reversal of the coordination mode of a pyridyl moiety, from the expected metal-nitrogen bonding mode to a cyclometalated coordination mode where a meta CH group in the same heterocyclic ring is deprotonated to generate a metal-carbon bond (Scheme 6.1a).[16] Rollover compounds have been predominantly described for bipyridine ligands coordinated to heavy atoms such as Pt(II) or Ir(III),[16, 17] and were extensively developed by the Zucca group.[18, 19] Recently, Hartinger et al. evaluated the anticancer abilities of a series of rollover cyclometalated bipyridine Pt(II) complexes, which appeared to be significantly influenced by the ancillary ligands.[20] Though Au(III) is isoelectronic to Pt(II) and shares the same popularity regarding cyclometalation, the synthesis of rollover cyclometalated Au(III) complexes have been rarely reported,[21, 22] and none of them have been studied in a biological context. In this work, we studied the coordination of two isomers of a tetrapyridyl ligand, *i.e.* (N6,N6'-di(isoquinolin-3-yl)-[2,2'-bipyridine]-6,6'-diamine (**H$_2$biqbpy1**) and N6,N6'-di(quinolin-2-yl)-[2,2'-bipyridine]-6,6'-diamine (**H$_2$biqbpy2**), to Au(III). Unexpectedly, in the same reaction conditions the former ligand led to the formation of the rollover bis-cyclometalated monocationic Au(III) complex **[1]Cl**, while the latter led to the tetrapyridyl coordination isomer, **[2]Cl**, which is characterized by deprotonated NH bridges and hence also a single positive charge (Scheme 6.1b). Both monocationic complexes were fully characterized, the reason for rollover was studied by DFT calculations, and the biological activities of the two compounds were compared. Our results demonstrate that rollover cyclometalation dramatically influenced the reactivity of the gold complex towards thiol groups, the selectivity of its cytotoxic properties, and its protein interactions.

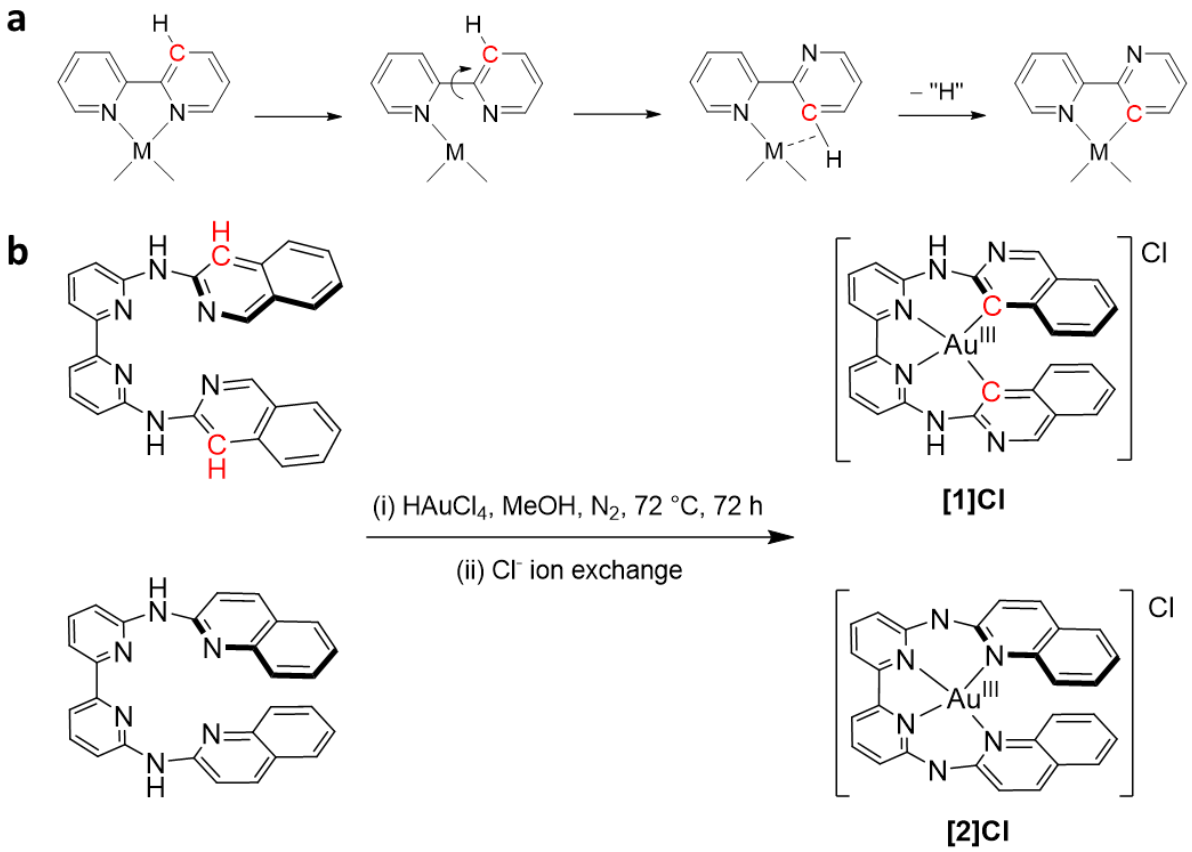

Scheme 6.1 *(a) Scheme for rollover cyclometalation.[19] (b) Synthesis route of isomer gold complexes* ***[1]Cl*** *and* ***[2]Cl****. Yields: 13% for* ***[1]Cl****, 18% for* ***[2]Cl****.*

6.2 Results and discussion

6.2.1 Synthesis. The ligands **H$_2$biqbpy1** and **H$_2$biqbpy2** were prepared according to the literature.[23] Upon refluxing for 3 days under N_2 a mixture of each ligand with one equivalent of $HAuCl_4$ in methanol, the gold complexes **[Au(biqbpy1)]$^+$** (**[1]$^+$**) and **[Au(biqbpy2)]$^+$** (**[2]$^+$**) were obtained after purification by silica column chromatography (Scheme 6.1b). The complexation of gold(III) to the ligands was confirmed via NMR. The ^{1}H NMR peak at 11.70 ppm (400 MHz, DMSO-d_6) demonstrated the protonation of the two secondary amine bridges of the ligand in **[1]$^+$**. By contrast, similar high-chemical shift peaks were not observed for **[2]$^+$**, suggesting at least partial deprotonation of the amine bridges. Next to these differences, the 2D-NMR analysis also provided strong evidence that **[1]$^+$** and **[2]$^+$** were coordinated following a different pattern. The ^{13}C-APT NMR showed that **[1]$^+$** had two quaternary carbon atoms more than **[2]$^+$**, indicating that **[1]$^+$** had two more Au-C bonds. It should be noticed that at that stage the ^{1}H NMR and ESI mass spectrometry did not yield insight in the nature of the counterion of these Au(III) complexes; probably, these samples had mixed counterions, *i.e.* $AuCl_4^-$, $AuCl_2^-$, and/or Cl^-.[24] Thus a chloride-loaded ion exchange resin was used to better define the nature of

the counter anion. **[1]Cl** was insoluble in water, while **[2]Cl** was quite hydrosoluble. Full characterization of the two compounds is given in the ESI.

6.2.2 X-ray crystallography and structure determination. Slow vapor diffusion of ethyl acetate into a methanol/DCM solution containing **[1]**$^+$ or **[2]**$^+$ gave red and black single crystals, respectively, suitable for X-ray crystal structure determination. The selected bond distances and angles are shown in Table AV1. The two crystal structures showed to contain different counter anions: one chloride anion per gold center for [**1**]$^+$, and one $AuCl_4^-$ complex anion per cationic gold complex for **[2]**$^+$. The compound **[1]Cl** crystallized in a monoclinic *P21/c* space group, while **[2](AuCl$_4$)** crystallized in a monoclinic *P21* space group. The cation of the two complexes showed a similar butterfly structure. The crystal structure of **[1]**$^+$ showed that it was a double "rollover" cyclometalated complex, characterized by a C^N^N^C coordination mode, while **[2]**$^+$ was a classical tetrapyridyl complex, characterized by a N^N^N^N coordination mode (Figure 6.1a). The M-C bond distances in **[1]**$^+$ (2.030(7)-2.060(5) Å) were similar to the M-N bond distances in **[2]**$^+$ (1.995(18)-2.081(18) Å). The two complexes exhibited distorted square-planar coordination spheres, as confirmed by the moderate tetradentate τ distortion values, *i.e.* τ = 0.19 for **[1]Cl** and τ = 0.21 for **[2](AuCl$_4$)** (τ = [360–(α+β)]/141, where α and β are the two greatest coordination angles of the tetradentate coordination sphere; τ = 0 reflects perfect planar coordination, τ = 1 indicates perfect tetrahedral coordination). Besides showing different coordination spheres, the two complexes were also characterized by significant differences in the geometry of their amine bridges. Clearly, in **[1]**$^+$, the bond distances in the bridge C9-N2, N2-C10, C19-N5 and N5-C20 fell within 1.348(10)-1.415(14) Å, indicative of a single bond character for both C-NH bonds. On the contrary, the amine-carbon bonds in **[2]**$^+$ were shorter, 1.331(7) and 1.40(3) Å, suggesting a higher double bond character for both amine-carbon bonds (C=N-C). This result suggested that the amine bridge in **[1]**$^+$ was protonated, while that in **[2]**$^+$ was deprotonated, thus generating conjugation between the lone pairs on the nitrogen bridges with the π system of the polypyridyl ligand. Last but not least, the highly distorted coordination sphere in both complexes generated a strongly helical structure, with both enantiomers being present as a 1:1 mixture in the crystal lattice because of the centrosymmetric space groups. In **[1]**$^+$ the quite similar helical structure, compared with **[2]**$^+$, was obtained due to the rollover cyclometallation. It was accompanied by a short centroid-centroid distance between rings A and I of the quinoline groups (Figure 6.1a, 3.982 Å for **[1]**$^+$, 3.343 Å for **[2]**$^+$), which is close to the typical π-π stacking distance of aromatic rings (3.4 Å),[25]

indicative of intramolecular π-π stacking between the two quinoline moieties in both complexes.

The prototypical molecular helices, helicenes, are organic compounds.[26, 27] However, metal-based molecular helices have been described by Lehn, Sauvage, and Hannon, for example.[28, 29] In this work, the helical structures of the gold complexes **[1]**$^+$ and **[2]**$^+$ indicate that gold complexation can be a new strategy to develop helical systems from planar ligands. In **[1]**$^+$ the perpendicular distances between the centroids of the terminal ring A and I to the least-squares plane defined by the central two pyridyl rings D and F (red characters in Figure 6.1a), was $d_{A\text{-}DF}$ = 1.946 Å and $d_{I\text{-}DF}$ = 1.586 Å, while in **[2]**$^+$ they were $d_{A\text{-}DF}$ = 1.984 Å and $d_{I\text{-}DF}$ = 1.040 Å (Figure 6.1b). The sum of the two values in **[1]**$^+$ ($\Sigma d_{A/I\text{-}DF}$ = 3.532) is about 17% larger than that in **[2]**$^+$ **(**$\Sigma d_{A/I\text{-}DF}$ = 3.024**)**, indicating a more helical geometry for the bis-cyclometalated complex **[1]**$^+$, possibly as a consequence of the repulsion between the terminal negatively charged carbon atoms. A difference in helical distortion was also found in the angle of the centroids of ring A and I with the Au(III) center ($\theta_{Au\text{-}AI}$). The $\theta_{Au\text{-}AI}$ of **[1]**$^+$ was 54.16°, which was larger than that in **[2]**$^+$ ($\theta_{Au\text{-}AI}$ = 46.66°), demonstrating again the larger distortion in **[1]**$^+$ than in **[2]**$^+$. Some gold(III) complexes have been shown to interact via supramolecular Au…Au bonds.[30] However, in the crystal lattice of **[1]Cl** and **[2](AuCl$_4$)**, the metal centers were too far from each other (d(Au…Au) ~ 4.2-5.5 Å) to suggest any aurophilic interactions. On the other hand, intermolecular π-π stacking occurs between the quinoline rings of two adjacent molecules (π-π distance around 3.9 Å in **[1]Cl**, Figure AV1), leading to an interesting supramolecular packing of the helices (Figure 6.1c). The crystal structure of **[2](AuCl$_4$)** showed slightly different supramolecular helical arrangements cut by the larger $AuCl_4^-$ counter anions, placed at a relatively short Au…Au distance (around 4.27 Å, Figure 6.1c). These packing differences are a probable consequence of the higher distortion of the coordination sphere in **[1]**$^+$ combined with the smaller size of chloride counter-anions, which leads to the generation of tighter intermolecular π-π stacking.

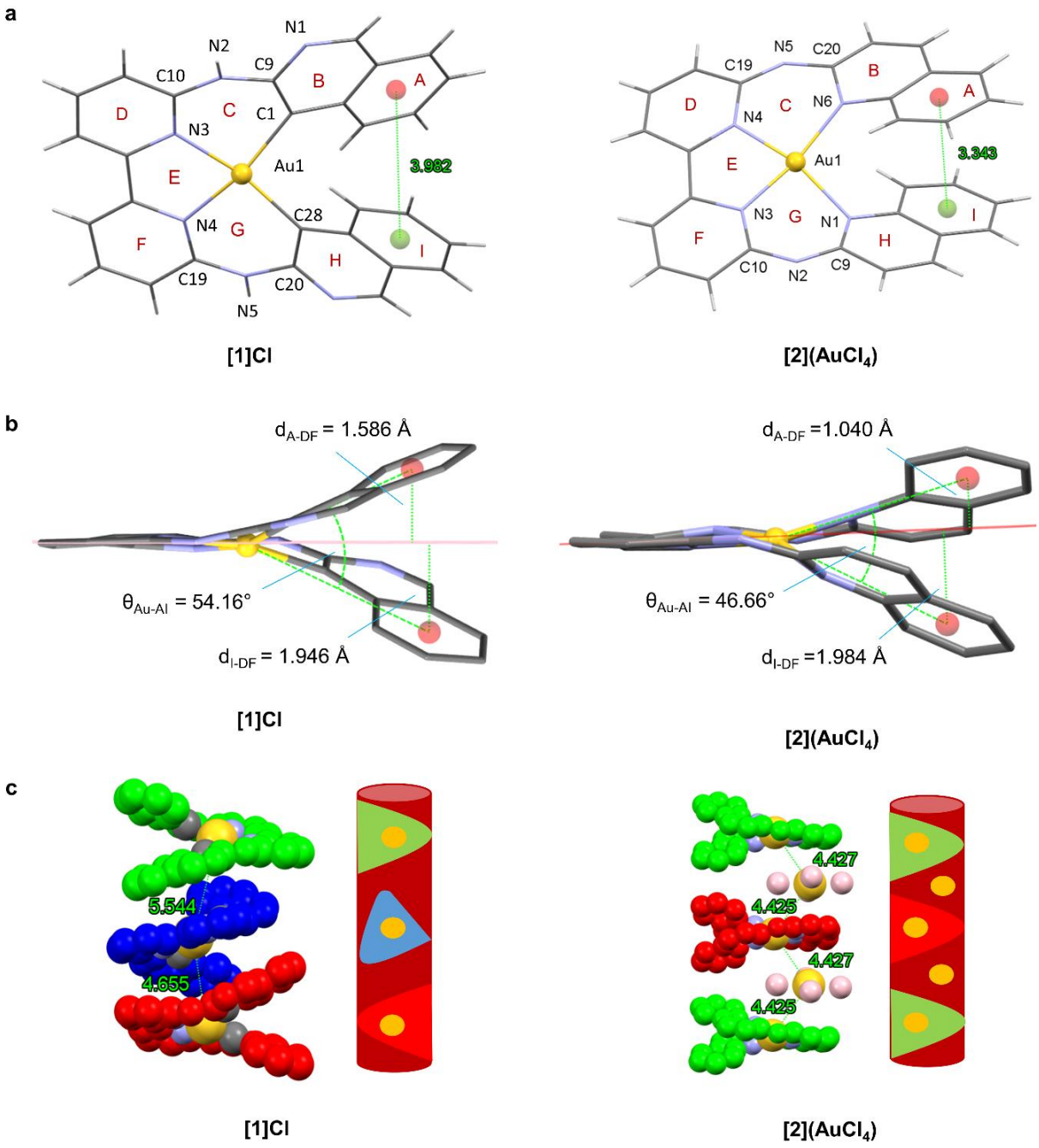

Figure 6.1 *(a) Cationic part and ring numbers (red characters) in the crystal structures (wireframe style) of gold complexes* ***[1]Cl*** *and* ***[2](AuCl$_4$)****. The counterions were omitted for clarity. (b) Selected angles (°) and distances (Å) in* ***[1]Cl*** *and* ***[2](AuCl$_4$)****. The least-squares plane defined by the rings D and F is shown as a red line. (c) Spacefill construction and schematic pictures of the supramolecular helices in the crystal structure of* ***[1]Cl*** *and* ***[2](AuCl$_4$)****. The Au atoms label in yellow color, Cl in pink, and the coordinated N in pale blue, coordinated C in grey, and non-coordinated C in green, dark blue, and red.*

6.2.3 DFT calculation of the classical and rollover complexes.

Considering the structural similarity between both ligands **H_2biqbpy1** and **H_2biqbpy2** and the different coordination modes obtained in **[1]**$^+$ and **[2]**$^+$ using identical reaction conditions, we investigated by DFT calculations what was the influence of rollover cyclometallation on the frontier orbitals of **[1]**$^+$ and the cause(s) of the rollover observed for **[1]**$^+$. As shown in Figure 6.2, both **[1]**$^+$ and **[2]**$^+$ show similar highly distorted coordination structures in the DFT minimized structures, with a short π-π distance on the centroid of the terminal ring of the quinoline groups (4.55 and 4.06 Å for **[1]**$^+$ and **[2]**$^+$, respectively, Table 6.1). The HOMO orbitals of both **[1]**$^+$ and **[2]**$^+$ have similar π symmetry, similar energies (-6.028 eV for **[1]**$^+$, -6.118 eV for **[2]**$^+$), and are both centered on the ligand with a negligible contribution of the Au(III) center (2.2% for **[1]**$^+$, 0% for **[2]**$^+$). By contrast, they show significantly different LUMO orbitals. The LUMO of **[1]**$^+$ was found centered on the bipyridine part of the ligand, while that of **[2]**$^+$ was essentially the expected anti-bonding combination of the Au(III) d_{x2-y2} orbitals (33%) and the p orbitals of the coordinated nitrogen atoms, which altogether results in drastically different LUMO energies (-2.520 eV for **[1]**$^+$ vs. -3.267 for **[2]**$^+$). Consequently, **[1]**$^+$ is predicted to be much more difficult to reduce than **[2]**$^+$, as expected for cyclometalated complexes. Besides, the HOMO-LUMO energy gaps of **[1]**$^+$ and **[2]**$^+$ is very different, *i.e.* 3.508 eV in **[1]**$^+$ and 2.611 eV in **[2]**$^+$, suggesting that both isomers should have different absorbance spectra. This hypothesis was further confirmed by time-dependent density functional theory calculations (TDDFT) in water, using COSMO to simulate solvent effects. As shown in Figure AV2, the classical N-bonded **[2]**$^+$ exhibited a red-shifted lowest-energy transition (694 nm), compared with that of the cyclometalated **[1]**$^+$ (451 nm).

To understand the reason for rollover cyclometallation we also simulated by DFT the tetrapyridyl coordination mode of **biqbpy1**$^{2-}$ (the isomer of **[1]**$^+$ called **[1a]**$^+$, Figure 6.2a) and the rollover cyclometalated binding mode of **biqbpy2**$^{2-}$ (the isomer of **[2]**$^+$ called **[2a]**$^+$, Figure 6.2b). In the rollover cyclometalated binding mode **[1]**$^+$ and **[2a]**$^+$, the HOMO and LUMO orbitals showed similar metal-independent π-symmetry and a LUMO located on the bipyridine ligand. The tetrapyridyl molecules **[2]**$^+$ and **[1a]**$^+$ shared similar metal-independent, π-symmetry HOMO orbitals; however, their LUMO orbitals was centered on the Au-N_4 antibonding $d_{x^2-y^2}$ – $p_{x,y}$ interaction, suggesting that upon reduction, coordination of the tetrapyridyl ligand to the metal might be weakened. Interestingly, the relative total binding energy of both cyclometalated molecules **[1]**$^+$ and **[2a]**$^+$ were found significantly lower than that of **[1a]**$^+$ and **[2]**$^+$ (Table 6.1). This result suggested that the thermodynamic stability of **[1]**$^+$

and **[2]**$^+$ might not be the only factor influencing which isomer is obtained in the reaction conditions, hence that both reactions were under kinetic control. However, it should also be noted that both hypothetical structures **[1a]**$^+$ and **[2a]**$^+$ show much longer centroid-centroid distances (6.70 and 7.29 Å, respectively) between the terminal rings of the quinolines, compared with that in the isomers obtained experimentally **[1]**$^+$ and **[2]**$^+$ (4.55 and 4.06 Å, respectively). This difference also suggests that intramolecular π-π stacking of the quinoline moieties may play an important role in the mechanism leading to the final structures, and hence in the occurrence of rollover cyclometalation for **[1]**$^+$.[19] Overall, a probable mechanism for the C-H activation of rollover **[1]**$^+$ is described in Figure 6.2c. Firstly, the precursor $HAuCl_4$ reacts with **H_2biqbpy1** to generate the first intermediumte **[Au(H2biqbpy1)Cl_2]Cl**, in which the Au(III) center bind with the bipyridine part and two chloride ligands. in a second step, intramolecular C-H…Cl hytrogen bond weakens the C-H bond, which triggers the generation of the first M-C bond and the second intermediumte **[Au(Hbiqbpy1)Cl]Cl**. Repeating this process a second time finally results in the rollover bis-cyclometalated **[1]Cl**.

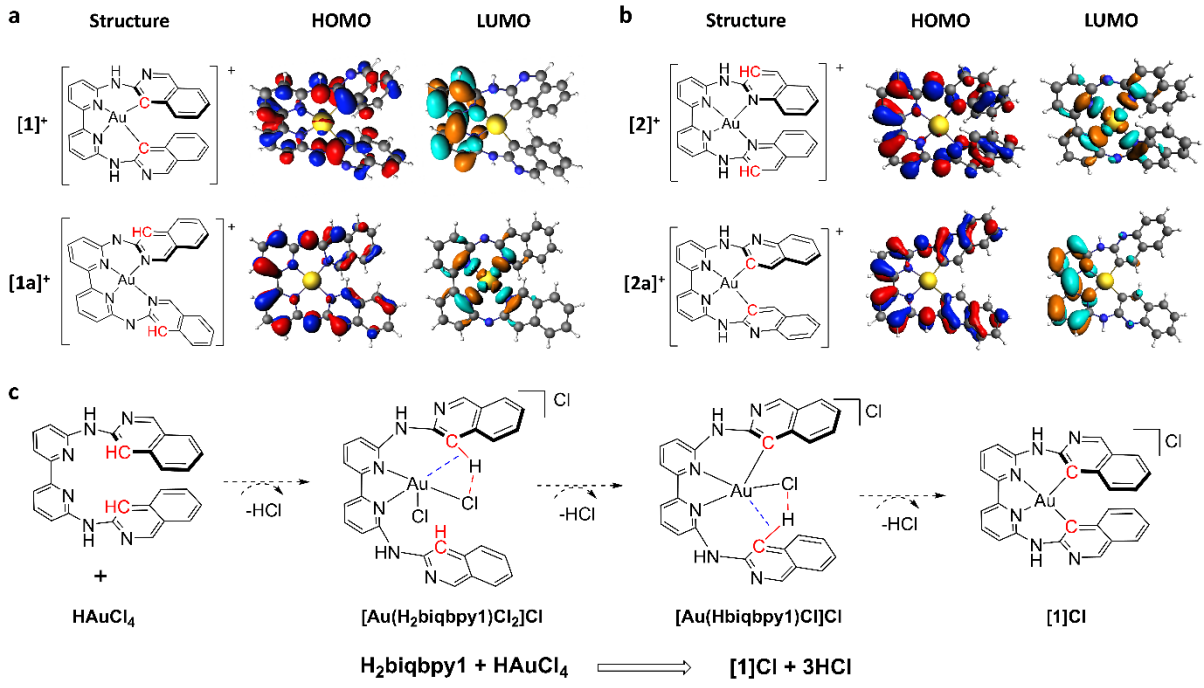

Figure 6.2 *Structure, calculated geometry, and frontier orbitals (HOMO, LUMO) of (a)* ***[1]***$^+$ *and* ***[1a]***$^+$*, (b)* ***[2]***$^+$ *and* ***[2a]***$^+$*. (c) Proposed mechanism for the C-H activation and cyclometalation of* H_2*biqbpy1 to form* ***[1]Cl****.*

Table 6.1. *The calculated information of complexes* ***[1]***$^{+}$, ***[2]***$^{+}$, ***[1a]***$^{+}$ *and* ***[2a]***$^{+}$.

Complex	HOMO (eV)	LUMO (eV)	ΔE (eV)	Relative total bind energy (eV)	End ring π-π distance (Å)
[1]$^{+}$	-6.028	-2.520	3.508	0	4.55
[2]$^{+}$	-6.118	-3.267	2.851	+0.8790	4.06
[1a]$^{+}$	-5.707	-3.096	2.611	+0.7726	6.70
[2a]$^{+}$	-6.332	-2.586	3.746	-0.6004	7.29

6.2.4 Behavior in solution. The absorbance spectra of both complexes in PBS solution at 310 K presented no significant changes over 24 h (Figure AV3), suggesting that they were thermally stable in aqueous solutions. **[2]Cl** had a significant intense metal-to-ligand charge transfer (MLCT) absorbance band around 450-500 nm, while that of **[1]Cl** was not remarkable, matching well with the trend observed by DFT and TDDFT calculation. However, when dissolving the complexes (50 μM) in PBS containing GSH (100 μM), the two complexes showed completely different behavior. The absorbance spectra of **[2]Cl** rapidly changed (in < 30 s), with a significant decrease of the absorption band in the visible region of the spectrum, which hereafter remained stable (for 25 min), while the spectrum of **[1]Cl** remained constant in these conditions (Figure 6.3a). The fast reaction of **[2]Cl** with GSH suggested that reduction of Au(III) to Au(I) might take place.[31] In order to check this, ^{1}H NMR was used to monitor the reaction between **[2]Cl** and GSH in D_2O, using a complex: GSH ratio of 1:2. After mixing GSH with **[2]Cl**, the ^{1}H NMR peaks of **[2]Cl** showed a dramatic change, accompanied by the generation of a peak for GSSG in the aliphatic region (2.98 and 3.26 ppm, blue star in Figure 6.3b). Although the peaks in the aromatic region can be split into two different Au(I) species involving the **H_2biqbpy2** ligand (indicated as yellow circle or green triangle in Figure 6.3b), their interpretation is difficult. After 24 h a precipitate was formed, which after filtration and ^{1}H NMR analysis was found to be the free tetrapyridyl ligand **(**Figure AV4**)**. These UV-vis and NMR spectroscopy experiments demonstrate that **[2]Cl** is easily reduced by GSH, while **[1]Cl** is much more stable in the presence of GSH, suggesting that the rollover cyclometalation stabilizes the gold complexes in thiol-containing solutions.

The stability of both complexes in cell-growing medium Opti-MEM complete (containing 2.5% fetal calf serum (FCS)) was also studied for 24 h using absorption spectroscopy (Figure 6.3c). For **[1]Cl** only the baseline of the spectrum increased gradually, suggesting the formation of nanoparticles might occur, but there was no obvious reaction nor isosbestic point. Nanoparticle

formation was confirmed by dynamic light scattering measurements (DLS, Figure 6.3d): the Opti-MEM solution of **[1]Cl** showed a significant signature of nanoparticles in the range 100-500 nm and much higher particle numbers than the Opti-MEM control group. By contrast, the absorbance band of **[2]Cl** in the visible region exhibited a rapid decrease during the first 10 min and finally disappeared, suggesting that a chemical reaction occurred in medium leading to a change of the Au coordination sphere. Considering the results above, reduction by thiol species present in the medium, like GSH, is the most likely explanation to the reaction of the Au(III) complex **[2]Cl** in medium. In summary, both experiments suggested that the Au(III) center in **[1]Cl** is stable to reduction by thiol groups such as GSH or FCS, proving that bis-cyclometalation results in the stabilization of gold(III), even if rollover cyclometallation is also accompanied by the formation of nanoparticles. By contrast, the gold(III) center in **[2]Cl** is very sensitive to reduction by thiol groups, which is a direct consequence of the high electronegativity and charge of the Au(III) center. In cell-growing medium, reduction of **[2]Cl** into Au(I) was followed by slow release of the insoluble tetrapyridyl ligand, with the concomitant formation of unidentified gold(I) species probably involving GSH.[32]

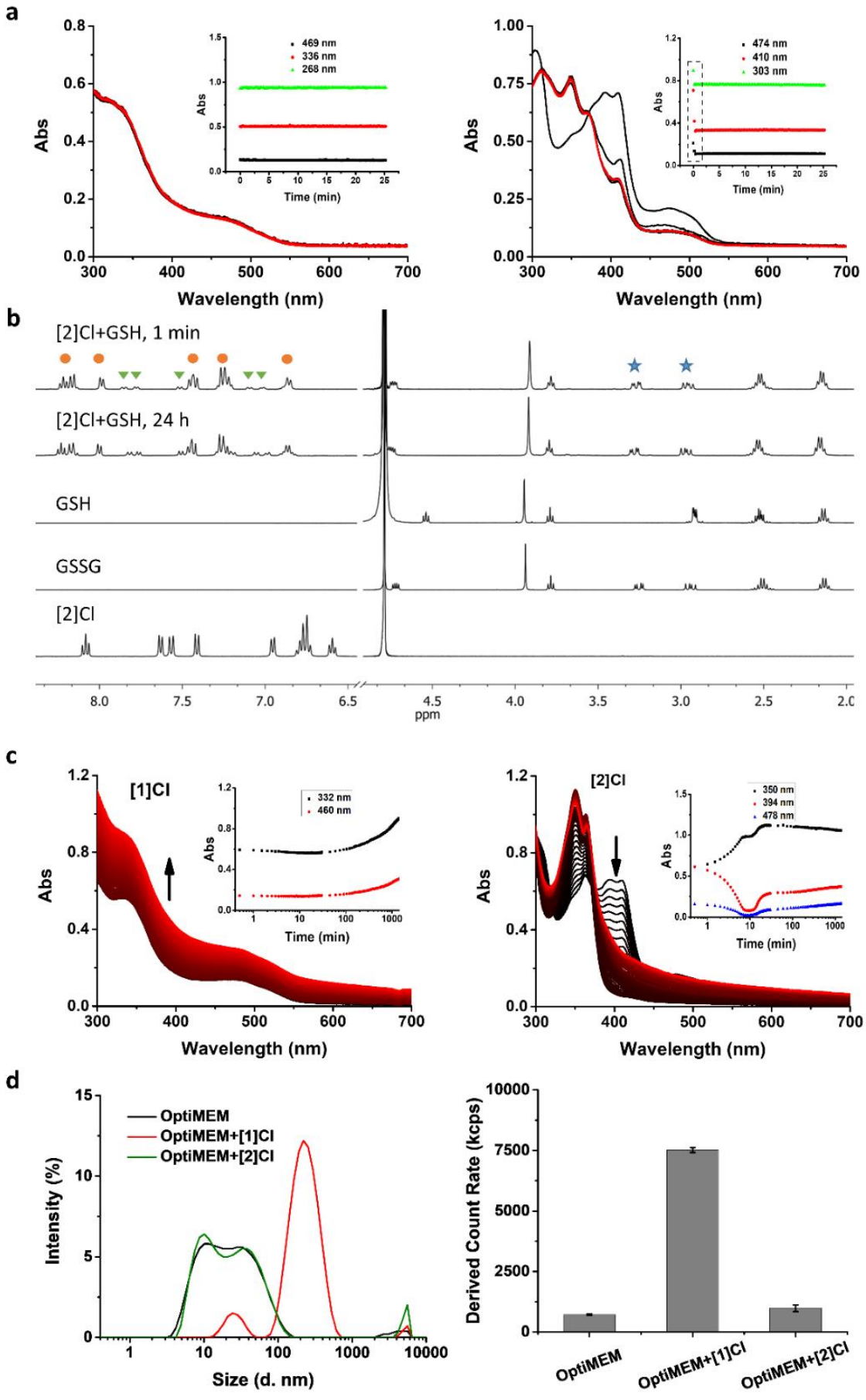
a
Abs
Wavelength (nm)
469 nm
336 nm
268 nm
Time (min)
474 nm
410 nm
303 nm
b
[2]Cl+GSH, 1 min
[2]Cl+GSH, 24 h
GSH
GSSG
[2]Cl
ppm
c
[1]Cl
332 nm
460 nm
[2]Cl
350 nm
394 nm
478 nm
d
OptiMEM
OptiMEM+[1]Cl
OptiMEM+[2]Cl
Intensity (%)
Size (d. nm)
Derived Count Rate (kcps)

Figure 6.3 *(a) Time evolution of the absorbance spectrum of* ***[1]Cl*** *and* ***[2]Cl*** *(50 μM) in PBS solution containing GSH (100 μM) for 25 min; measurement interval 12 s, color changes from black (0 s) to red (25 min). (b)* ^{1}*H NRM monitoring of a* ***[2]Cl****/GSH mixture in* D_2O *(concentration ratio 3 mM/6 mM). Yellow pie and green triangle indicate different Au(I) species. (c) Time evolution of the absorbance spectrum of* ***[1]Cl*** *and* ***[2]Cl*** *(50 μM) in Opti-MEM medium solution containing FCS (2.5% v/v) for 24 h; measurement interval: first 30 min every 0.5 min, the left 23.5 h every 15 min; color changes from black (0 s) to red (25 min). (d) DLS size distribution and derived count rate of* ***[1]Cl*** *and* ***[2]Cl*** *(50 μM) in Opti-MEM medium solution containing FCS (2.5% v/v).*

6.2.5 Anticancer properties. The cytotoxicity of both gold complexes **[1]Cl** and **[2]Cl** to 2D monolayers of four human cancer cell lines (lung cancer A549, skin cancer A431, melanoma cancer A375, and breast cancer MCF7) and one non-cancerous cell line (MRC5) was determined using a reported SRB assay, both in normoxic and hypoxic conditions.[33] The half-maximal effective concentrations (EC_{50} in μM), defined as the concentration necessary to kill 50% of the cells, compared to the untreated control, are shown in Table 6.2. The dose-response curves of gold complexes and cisplatin for these cells are shown in Figure AV5-7. Similar to cisplatin, **[1]Cl** showed a broad-spectrum anticancer ability to all cancer cells with EC_{50} in the range of 3.3-16 μM, both in normoxic and hypoxic conditions. Interestingly, **[1]Cl** exhibited a relatively higher EC_{50} (27 and 28 μM in normoxic and hypoxic conditions, respectively) to non-cancerous MRC5 cells, suggesting some form of selectivity towards cancer cells for **[1]Cl**. By comparison, **[2]Cl** showed generally lower EC_{50} values to cancer cells, *i.e.* higher cytotoxicity, with significant antiproliferative properties against A375 and MCF7 cancer cells (EC_{50} = 0.7 and 0.3 μM, respectively, in normoxic conditions). However, **[2]Cl** also showed high cytotoxicity to healthy MRC5 cells (3.3 and 1.5 μM in normoxic and hypoxic conditions, respectively), which might limit further applications in cancer treatment.

Apoptosis is a form of programmed cell death that can be induced by some metallodrugs. Here, the Annexin V/propidium iodide double staining was used to demonstrate if these two complexes kill cancer cells via the apoptosis or necrosis pathway. The different fluorescence states of both dyes in each cell indicates its status, i.e healthy (-/-), early apoptotic (+/-), later apoptotic (+/+) or necrotic (-/+). As shown in Figure 6.4a, after treatment with complex **[1]Cl** or **[2]Cl** (10 μM) to A549 cells for 24 h, the percentage of cells in the early and late apoptotic quadrants increased with compound concentration compared with the control group, suggesting that **[1]Cl** and **[2]Cl** kill A549 cells *via* stimulating the cell apoptosis process. Drug uptake

efficiency is highly relevant to the cytotoxicity of many metallodrugs. ICP-MS was hence used to determine the Au content in A549 cells. 24 h after treatment with these two complexes (1 µM), the Au content in A549 cells were 51 ng Au/million cells for **[1]Cl**, 8-fold higher than that of **[2]Cl** (6 ng Au/million cells, Figure 6.4b), demonstrating unambiguously the more efficient cellular uptake of cyclometalated rollover complex **[1]Cl** in A549 cells. Considering the identical charges of $\mathbf{[1]}^+$ and $\mathbf{[2]}^+$, this difference cannot be due here to increased passive uptake for **[1]Cl**, as usually hypothesized for cyclometalated complexes.[34] It might be due on the one hand to the formation of nanoparticles of **[1]Cl** in the cell medium, which may help to trigger energy-dependent endocytosis-related transport pathways. On the other hand, the lower uptake of **[2]Cl** might be linked to its decomposition in the cell culture into Au^+ ions that cannot be taken up efficiently, which also suggests that the toxicity of this complex might be that of the ligand **H_2biqbpy2**.

In humans, cancer appears as a 3D tumor characterized by a complicated microenvironment, which greatly influences the permeability, uptake, and cytotoxicity of anticancer drugs.[35] In recent years, *in vitro* 3D tumor spheroids have been developing as a more suitable model for the pre-screening of anticancer drugs, as they provide better mimicry of nutrient and drug penetration of *in vivo* tumors. Thus, the cytotoxicity of both gold complexes was also determined in 3D tumor spheroids, using the final spheroid diameter as well as a fluorescence-based Cell Titer Glo 3D end-point assay quantifying ATP (Figure 6.4c-e). [36] As shown in Figure 6.4c, **[1]Cl** showed good anti-proliferation properties in ~1000 µm diameter A549 tumor spheroids (EC_{50} = 7 µM), while **[2]Cl** exhibited slightly higher cytotoxicity (EC_{50} = 4 µM). Both were found less toxic than cisplatin (EC_{50} = 0.6 µM). Notably, the spheroid diameter was found not to be a good measure of the effect of these compounds, as the dose-diameter curves were found very different from the dose-response curves using the Cell TiterGlo3D assay. In summary, the cytotoxicity of the two gold complexes remained high in a 3D tumor model, where **[2]Cl** kept the higher cytotoxicity observed in a 2D model.

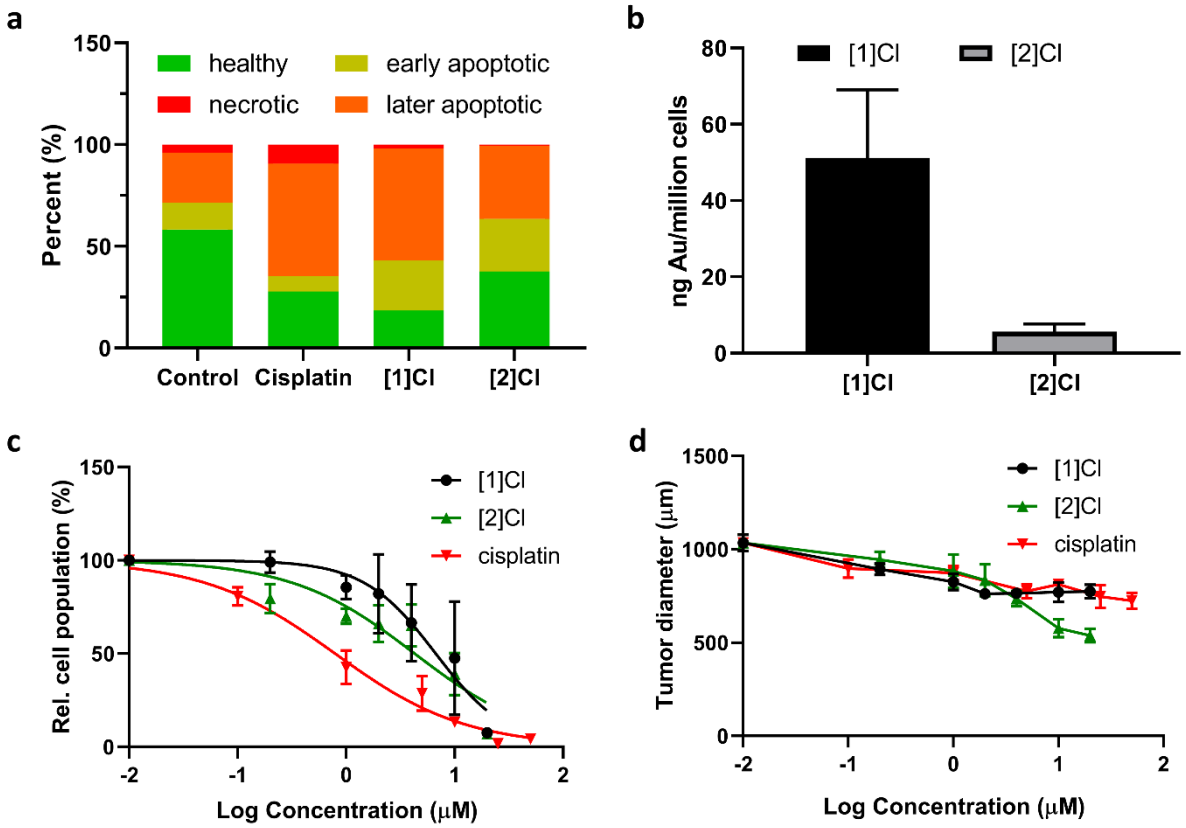

Figure 6.4 *(a) Flow cytometry quantification of healthy, early apoptotic, later apoptotic and necrotic A549 cells after treatment with cisplatin (15 μM),* ***[1]Cl*** *(10 μM) or* ***[2] Cl*** *(10 μM) for 24 h. (b) The Au content (ICP-MS) of A549 cells after treatment with* ***[1]Cl*** *and* ***[2]Cl*** *(1 μM) for 24 h. (c) 3D-tumor EC_{50} values of gold complexes and cisplatin based on a 3D CellTiterGlo ATP end-point assay. (d) Evolution of the tumor spheroid diameter after treatment with different concentrations of the gold complexes* ***[1]Cl*** *and* ***[2]Cl*** *or cisplatin.*

Table 6.2. *Half-maximal effective concentrations (EC_{50} in μM) of gold complexes* ***[1]Cl*** *and* ***[2]Cl*** *and cisplatin towards 2D cancer cell and healthy cell monolayers in normoxic (21% O_2) and hypoxic (1% O_2) conditions. 95% confidence interval (CI in μM over three independent biological experiments) are also indicated.*

Complex		**EC_{50} (μM)**											
		Cell line											
		A549	±CI	A431	±CI	A375	±CI	MCF7	±CI	MRC5	±CI	A549-3D	±CI
$[1]Cl_2$	Normoxic	3.3	+0.7 -0.6	4	+1 -1	5	+1 -1	4	+1 -1	27	+16 -9	7	+4 -2
	Hypoxic	5	+2 -2	16	+7 -5	6	+3 -2	9	+2 -1	28	+9 -6	N.D.	
[2]Cl	Normoxic	3.1	+0.3	3.5	+0.6	0.7	+0.2	0.3	+0.1	3.3	+0.8	4	+3

			-0.3		-0.5		-0.1		-0.1		-0.7		-2
	Hypoxic	3.9	+0.7 -0.6	2.9	+0.8 -0.5	4	+4 -2	2.1	+0.1 -0.1	1.5	+0.2 -0.2	N.D.	
cisplatin	Normoxic	4.5	+0.7 -0.6	1.8	+0.5 -0.4	1.2	+0.1 -0.1	3.6	+1.2 -0.9	5.8	+1.5 -1.2	0.8	+0.3 -0.2
	Hypoxic	24	+11 -5	13	+4 -3	3.4	+0.8 -0.7	N.D.		9.4	+5.7 -3.6	N.D.	

6.2.6 Proteins binding and inhibition properties. Several gold complexes have been demonstrated to show significant binding and inhibition properties to several proteins, such as urease,[37] aquaporin,[38] and particularly TrxR.[9, 32] To determine the inhibition properties of **[1]Cl** and **[2]Cl** towards mammalian TrxR, a spectrophotometric assay was realized using commercially available rat-liver TrxR. As shown in Table 6.3, **[1]Cl** did not show any inhibition activity to TrxR at the tested concentration. This low inhibition property might be attributed to the weak reactivity of **[1]Cl** with biological thiols (see above). By contrast, **[2]Cl** showed significant TrxR inhibition activity with a submicromolar IC_{50} (0.13 ± 0,02 µM), which may be attributed to its high reactivity with reducing thiols, which generate Au^+ ions that are known inhibitors of TxrR. The significant difference between **[1]Cl** and **[2]Cl** indicates that rollover cyclometalation might represent a promising design strategy to generate anticancer gold compounds that show a target different from TxrR, and do not release polypyridyl ligands upon reacting with cell medium or intracellular GSH.

Indeed, next to releasing Au^+ ions, reduction of **[2]Cl** by biological thiols also leads to the release of the free polypyridyl ligand **H_2biqbpy2**, which might have unselective toxicity. This hypothesis stimulated us to look into the biological activity of the two polypyridyl ligands **H_2biqbpy1** and **H_2biqbpy2**. N-heterocyclic ligands are found in roughly 60% of FDA-approved drugs, and pyridine ring systems are prominent examples of such fragments.[39] Many N-heterocyclic ligands have been considered as potential inhibitors of potassium channels in the cell membrane or mitochondrial membrane.[40-42] Potassium channels have been proposed as emerging targets in cancer therapy, for their overexpression in several cancer cell lines, and their specific functions in cell proliferation as they control cell cycle progression.[43, 44] On the other hand, a classical safety issue in medicinal chemistry is K^+ channel inhibition, in particular the broad-substrate $K_v11.1$ (hERG) potassium channel, which is known to generate cardiac toxicity *in vivo*.[45, 46] Here, we evaluated the $K_v11.1$ channel interaction of the two gold complexes **[1]Cl** and **[2]Cl** and their ligands **H_2biqbpy1** and **H_2biqbpy2** at a single

concentration (10 μM) in a [^{3}H]dofetilide displacement assay.[47] When a compound binds to the K_v11.1 channel, the binding of reference hERG blocker [^{3}H]dofetilide is decreased, which is used to quantify the K_v11.1 binding efficiency of the tested compounds. As shown in Table 3, all four compounds displaced [^{3}H]dofetilide from the channel albeit to different degrees. While **H$_2$biqbpy1** was a poor binder, **H$_2$biqbpy2** displaced 84% of [^{3}H]dofetilide binding. The gold complexes showed a (slightly) higher effect, *i.e.* 91% displacement for the rollover compound **[1]Cl** and 92% displacement for **[2]Cl**. Such good K^+-channel binding properties of both metal complexes are probably due to the high similarity, both in terms of shape and positive charge, of these molecules. Altogether, both **[1]Cl** and **[2]Cl** efficiently bind to the K_v11.1 channel. The higher toxicity of **[2]Cl** might be related to a combination between K^+ channel inhibition by the released ligand, and TrxR inhibition by the released Au^+ ions.

Table 6.3. *Binding of tetrapyridyl ligands and their gold(III) complexes to TrxR and K_v11.1 proteins.*

Compound	TrxR inhibition IC_{50} (μM)	[^{3}H]dofetilide binding remaining (%)[b]	K_v11.1 binding (%)[c]
H$_2$biqbpy1	N.D.[a]	64±4	36±4
[1]Cl	>5	8.7±0.1	91.3±0.1
H$_2$biqbpy2	N.D.	16±4	84±4
[2]Cl	0.13±0.02	7.9±0.2	92.1±0.2

[a] N.D. = not determined. [b] tested concentration = 10 μM; [c] K_v11.1 binding (%) = 100%-[^{3}H]dofetilide binding remain (%).

6.3 Discussion and Conclusion

Many gold(III) compounds have been demonstrated to be potential anticancer metallodrugs due to their easy reduction to gold(I) upon intracellular uptake. Gold(I) species always show strong binding affinity to the thiol groups of many key biomolecules and enzymes inside a cell, notably to glutathione (GSH) or thioredoxin reductase (TrxR), which are overexpressed in cancer cells because they control the redox balance of cells.[10, 48, 49] However, several cyclometalated gold(III) complexes have been shown to withstand reduction by biological thiols while keeping anticancer properties, indicating that a different anticancer mechanism may be operative.[50] Very limited research has focused on the comparison of cyclometalated *vs.* classical nitrogen-coordinated gold compounds, both from the chemical structure point of view to that of the biological activities. In this work, we synthesized two gold(III) isomers, *i.e.* the rollover cyclometalated **[1]Cl** (C^N^N^C) and the classically nitrogen-coordinated **[2]Cl** (N^N^N^N). The two complexes show strikingly similar helical molecular structures, but they exhibited dramatically different reactivity to GSH and TrxR proteins: **[1]Cl** shows no reaction to thiol

groups and no TxrR inhibition, while **[2]Cl** reacts with thiol groups rather quickly, which is accompanied with the release of the tetradentate ligand and TxrR-inhibiting Au^+ ions. The low thiol group susceptibility of **[1]Cl** should be attributed to the high stability of the M-C bond and localization of the LUMO of this complex on the bipyridine group, without the involvement of metal.

In biological terms, both compounds were found anticancer active, but in a quite different manner. On the one hand, **[2]Cl** is an interesting cytotoxic compound that upon reduction releases both a TxrR-inhibiting Au^+ ion and a good K^+-channel blocker ligand **H_2biqbpy2**, which may act synergistically. However, cellular uptake is limited by thiol-induced decomposition outside the cells, and toxicity to non-cancerous cells is also high. On the other hand, **[1]Cl** is more promising in several aspects: it shows much higher toxicity in cancerous *vs.* non-cancerous cell lines, and a high cellular uptake probably in the form of nanoparticles. Cellular uptake provides intact Au(III) complexes inside the cell that have excellent redox stability in presence of biological thiols, and improved K^+ channel binding, compared to the ligand **H_2biqbpy1**. It is unclear at present if K^+ channel inhibition is the reason for the higher toxicity to cancer cells. However, bis-cyclometalation appears as an appealing strategy to generate Au(III) anticancer compounds that enter the cell efficiently and inhibit proteins that are different from TxrR.

6.4 Experimental section

The DFT calculation, cell culture, cytotoxicity, cell uptake, apoptosis and 3D tumor spheroids inhibition experiments were carried out according to the description in chapters 3 and 4.

6.4.1 Synthesis and analytical data for ligands and gold complexes

H_2biqbpy1.

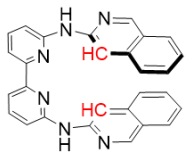

H_2biqbpy1

This ligand was synthesized according to a literature procedure.[1] A mixture of 6,6'-dibromo-2,2'-bipyridine (1004 mg, 3.18 mmol), $Pd(dba)_2$ (296 mg, 0.32 mmol), racemic BINAP (395 mg, 0.64 mmol) and cesium carbonate (4145 mg, 12.14 mmol) was partially dissolved in dry toluene (50 mL) under N_2 atmosphere. The mixture was stirred for 10 min, then 3-aminoisoquinoline (919 mg, 6.37 mmol) was added, followed by heating the reaction mixture to 85 °C. After 3 days of stirring, the brown mixture was cooled down. Demi water (75.0 mL) was added and the mixture was stirred for 1 h. The mixture was then filtered, and dry in a vacuum to obtain the light green product (1288 mg, 91% yield). **ESI-MS** (cation): m/z calcd 441.2 ($C_{28}H_{20}N_6$ + H^+), found

441.2. **^{1}H NMR** (300 MHz, DMSO-d_6): δ 10.00 (s, 2H), 9.13 (s, 2H), 8.80 (s, 2H), 8.08 – 7.98 (m, 4H), 7.94 (t, *J* = 7.8 Hz, 2H), 7.83 (t, *J* = 8.4 Hz, 2H), 7.67 (t, *J* = 7.4 Hz, 2H), 7.43 (t, *J* = 7.3 Hz, 2H), 7.35 (d, *J* = 7.9 Hz, 2H).

H_2biqbpy2.

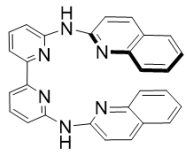

H_2biqbpy2

The synthesis of H_2biqbpy2 is similar to that of H_2biqbpy1, except that 2-aminoquinoline was used to replace 3-aminoisoquinoline. The yield is 943 mg, 2.14 mmol, 67%. **ESI-MS** (cation): m/z calcd 441.2 ($C_{28}H_{20}N_6$ + H^+), found 441.2. **^{1}H NMR** (300 MHz, DMSO): δ 10.15 (s, 2H), 8.46 (dd, *J* = 7.5, 1.7 Hz, 2H), 8.22 (d, *J* = 9.0 Hz, 2H), 8.04 – 7.90 (m, 4H), 7.80 (td, *J* = 9.1, 8.7, 1.8 Hz, 6H), 7.64 (ddd, *J* = 8.4, 6.9, 1.5 Hz, 2H), 7.38 (ddd, *J* = 8.1, 6.9, 1.3 Hz, 2H).

[Au(biqbpy1)]Cl ([1]Cl).

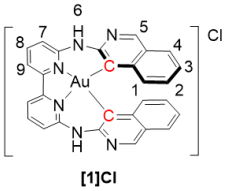

[1]Cl

A mixture of H_2biqbpy1 (100 mg, 0.23 mmol) and $HAuCl_4$ (85 mg, 0.25 mmol) was dissolved in MeOH (30 mL), and stirred under N_2 atmosphere at 75 °C for 3 days. Then the solvent was rotary evaporated. The crude product obtained was purified by silica chromatography using dichloromethane-MeOH mixtures (10:2, R_f = 0.35) as eluent to afford the target compound. Then the complex was dissolved in the MeOH and across the Cl^- ion exchange resin to unify the counterion as Cl^-. The yield of final product **[1]Cl** was 25 mg, 0.03 mmol, 13%. HRMS (cation): m/z calcd 635.1258 ($[C_{28}H_{18}AuN_6]^+$), found 635.1244. **^{1}H NMR** (400 MHz, DMSO-d_6): δ 11.70 (s, 2H, H^6), 9.08 (d, *J* = 0.7 Hz, 2H, H^5), 8.25 (dd, *J* = 8.4, 7.5 Hz, 2H, H^8), 8.19 (dd, *J* = 7.6, 1.1 Hz, 2H, H^9), 7.87 (dd, *J* = 8.4, 1.1 Hz, 2H, H^7), 7.78 (dt, *J* = 8.0, 1.0 Hz, 2H, H^4), 7.29 (dd, *J* = 8.6, 1.0 Hz, 2H, H^1), 7.09 (ddd, *J* = 8.0, 6.8, 1.1 Hz, 2H, H^3), 6.84 (ddd, *J* = 8.4, 6.9, 1.4 Hz, 2H, H^2). **^{13}C NMR** (101 MHz, DMSO-*d6*): δ 153.10, 151.91, 148.04, 141.22, 140.81, 139.21, 129.38, 128.91, 127.24, 126.25, 125.28, 116.34, 115.44, 113.03. **Elemental analysis**: calcd for **[1]Cl** + $4H_2O$: C 45.27, H 3.53, N 11.31; found C 45.49, H 3.63, N 11.29.

[Au(biqbpy2)]Cl ([2]Cl).

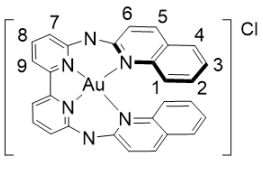

[2]Cl

A mixture of H_2biqbpy2 (100 mg, 0.23 mmol) and $HAuCl_4$ (85 mg, 0.25 mmol) was dissolved in MeOH (30 mL), and stirred under N_2 atmosphere at 75 °C for 72 h. Then the solvent was rotary evaporated. The crude product obtained was purified by silica chromatography using dichloromethane-MeOH mixtures (10:1, R_f = 0.3) as eluent to afford the target compound. Then the complex was dissolved in the MeOH and across the Cl^- ion exchange resin to unify the

counterion as Cl^-. The yield of final product **[2]Cl** was 27 mg, 0.04 mmol, 18%. **HRMS** (cation): m/z calcd 635.1258 ($[C_{28}H_{18}AuN_6]^+$), found 635.1236. **^{1}H NMR** (400 MHz, DMSO-*d6*): δ 8.21 (dd, *J* = 8.4, 7.4 Hz, 2H, H^8), 8.10 (dd, *J* = 7.5, 1.3 Hz, 2H, H^7), 7.96 (d, *J* = 8.9 Hz, 2H, H^5), 7.63 (dd, *J* = 8.4, 1.2 Hz, 2H, H^9), 7.59 – 7.52 (m, 2H, H^2), 7.41 – 7.34 (m, 2H, H^4), 7.28 (d, *J* = 8.9 Hz, 2H, H^6), 6.98 – 6.88 (m, 4H, H^3. H^1). **^{1}H NMR** (400 MHz, D_2O): δ 7.99 (t, *J* = 8.4, 7.4 Hz, 2H, H^8), 7.49 (d, *J* = 7.7, 1.2 Hz, 2H, H^7), 7.45 (d, *J* = 8.9 Hz, 2H, H^6), 7.30 (d, *J* = 8.3, 1.1 Hz, 2H, H^9), 6.83 (d, 2H, H^3), 6.70 – 6.54 (m, 6H, H^4, H^5, H^1), 6.47 (t, *J* = 7.3 Hz, 2H, H^2). **^{13}C NMR**, (101 MHz, D_2O): 175.78, 152.50, 149.51, 142.01, 140.66, 139.92, 129.11, 128.65, 126.46, 125.70, 125.57, 122.93, 118.65, 116.89. **Elemental analysis**: calcd for **[2]Cl** + $4H_2O$: C 45.27, H 3.53, N 11.31; found C 45.26, H 3.51, N 11.30.

6.4.2 Proteins binding and inhibition properties of gold complexes

TrxR inhibition property determination. To determine the inhibition of mammalian thioredoxin reductase (TrxR), a spectrophotometric assay was done using commercially available rat liver TrxR (Sigma-Aldrich). The enzyme was diluted with distilled water to achieve a concentration of 2.5 U/mL. The gold complexes were freshly dissolved DMF to get a stock solution of 10 mM. To a 25 µL aliquot of the enzyme solution, 25 µL of potassium phosphate buffer, pH 7.0, containing the complexes at different concentrations or vehicle (DMF) without compounds (control probe) was added, and the resulting solutions (final concentration of DMF: max. 0.5% v/v) were incubated with moderate shaking for 75 min at 37 °C in a 96-well plate. Subsequently, to each well, 225 µL of the reaction mixture (1000 µL of reaction mixture consisted of 500 µL of potassium phosphate buffer, pH 7.0, 80 µL of EDTA solution (100 mM, pH 7.5), 20 µL of BSA solution (0.2%), 100 µL of NADPH solution (20 mM), and 300 µL of distilled water) was added. The reaction was started by the addition of 25 µL of an ethanolic 5,5'-Dithiobis 2-nitrobenzoic solution (DTNB, 20 mM). After proper mixing, the formation of 5-TNB was monitored with a microplate reader (Perkin-Elmer Victor X4) at 405 nm in 10 s intervals for 10 min. The increase in 5-TNB concentration over time followed a linear trend ($R^2 \geq 0.99$), and the enzymatic activities were calculated as the slopes (increase in absorbance per second) thereof. For each tested compound, the noninterference with the assay components was confirmed by a negative control experiment using an enzyme-free solution. The IC_{50} values were calculated as the concentration of complexes decreasing the enzymatic activity of the untreated control by 50% and are given as the means and standard deviations of two independent experiments.

K_v11.1 potassium channel binding affinity. This experiment was carried out according to a literature procedure.[42] Briefly, the cell membrane of HEK293Kv 11.1 cells was collected. Then the loading of [^{3}H]dofetilide on the cell membrane was performed by mixing membrane aliquots containing 30 µg protein with 2 nM [^{3}H]dofetilide in a total volume of 100 µL incubation buffer at 15 °C for 90 min. After loading, a single point dissociation assay was initiated by the addition of 10 µM dofetilide in the absence (control) or presence of 10 µM of gold complexes and corresponding ligands. After 10 min of incubation, samples were separated by rapid filtration through a 96-well GF/B filter plate using a Perkin Elmer Filtermate-harvester (Perkin Elmer, Groningen, The Netherlands). Filters were subsequently washed with ice-cold wash buffer two times. Then the filter-bound radioactivity was determined by scintillation spectrometry *via* the 1450 Microbeta Wallac Trilux scintillation counter (Perkin Elmer) after the addition of 37.5 µL Microscint and for another 2 h extraction. The binding of [^{3}H]astemizole in the control was set as 100%.

6.5 References

1. F. M. Muggia, A. Bonetti, J. D. Hoeschele, M. Rozencweig and S. B. Howell, *J. Clin. Oncol*, 2015, **33**, 4219-4226.
2. Y. R. Liu, C. Ji, H. Y. Zhang, S. X. Dou, P. Xie, W. C. Wang and P. Y. Wang, *Arch. Biochem. Biophys.*, 2013, **536**, 12-24.
3. S. Nafisi and N. Zeinab, *DNA Cell Biol.*, 2009, **28**, 469-477.
4. M. Pandrala, M. K. Sundaraneedi, A. J. Ammit, C. E. Woodward, L. Wallace, F. R. Keene and J. G. Collins, *Eur. J. Inorg. Chem.*, 2015, **34**, 5694-5701.
5. S. M. Meier-Menches, C. Gerner, W. Berger, C. G. Hartinger and B. K. Keppler, *Chem. Soc. Rev.*, 2018, **47**, 909-928.
6. S. Thota, D. A. Rodrigues, D. C. Crans and E. J. Barreiro, *J. Med. Chem.*, 2018, **61**, 5805-5821.
7. T. Lazarević, A. Rilak and Ž. D. Bugarčić, *Eur. J. Med. Chem.*, 2017, **142**, 8-31.
8. N. Cutillas, G. S. Yellol, C. de Haro, C. Vicente, V. Rodríguez and J. Ruiz, *Coord. Chem. Rev.*, 2013, **257**, 2784-2797.
9. M. Mora, M. C. Gimeno and R. Visbal, *Chem. Soc. Rev.*, 2019, **48**, 447-462.
10. T. Zou, C. T. Lum, C.-N. Lok, J.-J. Zhang and C.-M. Che, *Chem. Soc. Rev.*, 2015, **44**, 8786-8801.
11. J.-J. Jia, W.-S. Geng, Z.-Q. Wang, L. Chen and X.-S. Zeng, *Cancer Chemother. Pharmacol.*, 2019, **84**, 453-470.
12. M. P. Gamcsik, M. S. Kasibhatla, S. D. Teeter and O. M. Colvin, *Biomarkers*, 2012, **17**, 671-691.
13. F. Angelucci, A. A. Sayed, D. L. Williams, G. Boumis, M. Brunori, D. Dimastrogiovanni, A. E. Miele, F. Pauly and A. Bellelli, *J. Biol. Chem.*, 2009, **284**, 28977-28985.
14. I. Ott, *Coord. Chem. Rev.*, 2009, **253**, 1670-1681.
15. R. Kumar and C. Nevado, *Angew. Chem. Int. Ed.*, 2017, **56**, 1994-2015.
16. B. Butschke and H. Schwarz, *Chem. Sci.*, 2012, **3**, 308-326.
17. M. Leist, C. Kerner, L. T. Ghoochany, S. Farsadpour, A. Fizia, J. P. Neu, F. Schön, Y. Sun, B. Oelkers, J. Lang, F. Menges, G. Niedner-Schatteburg, K. S. M. Salih and W. R. Thiel, *J. Organomet. Chem.*, 2018, **863**, 30-43.
18. A. Zucca, G. L. Petretto, S. Stoccoro, M. A. Cinellu, M. Manassero, C. Manassero and G. Minghetti, *Organometallics*, 2009, **28**, 2150-2159.
19. L. Maidich, G. Dettori, S. Stoccoro, M. A. Cinellu, J. P. Rourke and A. Zucca, *Organometallics*, 2015, **34**, 817-828.
20. M. V. Babak, M. Pfaffeneder-Kmen, S. M. Meier-Menches, M. S. Legina, S. Theiner, C. Licona, C. Orvain, M. Hejl,

M. Hanif, M. A. Jakupec, B. K. Keppler, C. Gaiddon and C. G. Hartinger, *Inorg. Chem.*, 2018, **57**, 2851-2864.

21. L. Maidich, M. A. Cinellu, F. Cocco, S. Stoccoro, M. Sedda, S. Galli and A. Zucca, *J. Organomet. Chem.*, 2016, **819**, 76-86.
22. F. Cocco, M. A. Cinellu, G. Minghetti, A. Zucca, S. Stoccoro, L. Maiore and M. Manassero, *Organometallics*, 2010, **29**, 1064-1066.
23. V. H. S. van Rixel, B. Siewert, S. L. Hopkins, S. H. C. Askes, A. Busemann, M. A. Siegler and S. Bonnet, *Chem. Sci.*, 2016, **7**, 4922-4929.
24. Y. Simonov, O. Bologa, P. Bourosh, N. Gerbeleu, J. Lipkowski and M. Gdaniec, *Inorg. Chim. Acta*, 2006, **359**, 721-725.
25. C. Janiak, *Dalton Trans.*, 2000, **21**, 3885-3896.
26. Y. Nakakuki, T. Hirose and K. Matsuda, *J. Am. Chem. Soc.*, 2018, **140**, 15461-15469.
27. N. Saleh, C. Shen and J. Crassous, *Chem. Sci.*, 2014, **5**, 3680-3694.
28. G. W. Coates, P. D. Hustad and S. Reinartz, *Angew. Chem. Int. Ed.*, 2002, **41**, 2236-2257.
29. R. Kramer, J. M. Lehn and A. Marquis-Rigault, *Proc. Natl. Acad. Sci. U.S.A.*, 1993, **90**, 5394-5398.
30. Q. Wan, J. Xia, W. Lu, J. Yang and C.-M. Che, *J. Am. Chem. Soc.*, 2019, **141**, 11572-11582.
31. K. K. Kung, H. M. Ko, J. F. Cui, H. C. Chong, Y. C. Leung and M. K. Wong, *Chem. Commun.*, 2014, **50**, 11899-11902.
32. T. Zou, C. T. Lum, S. S. Chui and C. M. Che, *Angew. Chem. Int. Ed.*, 2013, **52**, 2930-2933.
33. X. Q. Zhou, A. Busemann, M. S. Meijer, M. A. Siegler and S. Bonnet, *Chem. Commun.*, 2019, **55**, 4695-4698.
34. H. Huang, P. Zhang, H. Chen, L. Ji and H. Chao, *Chem. Eur. J*, 2015, **21**, 715-725.
35. J. Karges, S. Kuang, F. Maschietto, O. Blacque, I. Ciofini, H. Chao and G. Gasser, *Nat. Commun.*, 2020, **11**, 3262.
36. X. Q. Zhou, M. Xiao, V. Ramu, J. Hilgendorf, X. Li, P. Papadopoulou, M. A. Siegler, A. Kros, W. Sun and S. Bonnet, *J. Am. Chem. Soc.*, 2020, **142**, 10383-10399.
37. L. Mazzei, M. N. Wenzel, M. Cianci, M. Palombo, A. Casini and S. Ciurli, *ACS Med. Chem. Lett.*, 2019, **10**, 564-570.
38. A. de Almeida, A. F. Mosca, D. Wragg, M. Wenzel, P. Kavanagh, G. Barone, S. Leoni, G. Soveral and A. Casini, *Chem. Commun.*, 2017, **53**, 3830-3833.
39. M. Meanwell, M. B. Nodwell, R. E. Martin and R. Britton, *Angew. Chem. Int. Ed.*, 2016, **55**, 13244-13248.
40. L. P. Du, K. C. Tsai, M. Y. Li, Q. D. You and L. Xia, *Bioorg. Med. Chem. Lett.*, 2004, **14**, 4771-4777.
41. J. F. Carvalho, J. Louvel, M. L. Doornbos, E. Klaasse, Z. Yu, J. Brussee and I. J. AP, *J. Med. Chem.*, 2013, **56**, 2828-2840.
42. Z. Yu, J. P. van Veldhoven, J. Louvel, I. M. t Hart, M. B. Rook, M. A. van der Heyden, L. H. Heitman and I. J. AP, *J. Med. Chem.*, 2015, **58**, 5916-5929.
43. A. Felipe, R. Vicente, N. Villalonga, M. Roura-Ferrer, R. Martinez-Marmol, L. Sole, J. C. Ferreres and E. Condom, *Cancer Detect. Prev.*, 2006, **30**, 375-385.
44. L. A. Pardo and W. Stuhmer, *Nat. Rev. Cancer*, 2014, **14**, 39-48.
45. P. Feng, L. Zhao, F. Guo, B. Zhang, L. Fang, G. Zhan, X. Xu, Q. Fang, Z. Liang and B. Li, *Chem. Biol. Interact.*, 2018, **293**, 115-123.
46. K. Jeevaratnam, K. R. Chadda, C. L. Huang and A. J. Camm, *J. Cardiovasc. Pharmacol. Ther.*, 2018, **23**, 119-129.
47. Z. Yu, J. P. D. van Veldhoven, I. M. E. t Hart, A. H. Kopf, L. H. Heitman and A. P. Ijzerman, *Eur. J. Med. Chem.*, 2015, **106**, 50-59.
48. K. Nakao, N. Minato and S. Uemoto, *Innovative medicine: basic research and development*, Springer Nature, 2015.
49. A. Ilari, P. Baiocco, L. Messori, A. Fiorillo, A. Boffi, M. Gramiccia, T. Di Muccio and G. Colotti, *Amino Acids*, 2012, **42**, 803-811.
50. S. Gukathasan, S. Parkin and S. G. Awuah, *Inorg. Chem.*, 2019, **58**, 9326-9340.